How to cite: *Angew. Chem. Int. Ed.* **2022,** *61,* e202200781
International Edition: doi.org/10.1002/anie.202200781
German Edition: doi.org/10.1002/ange.202200781

Porphyrinoids

Helicity Modulation in NIR-Absorbing Porphyrin-Ryleneimides

*Shivaprasad Achary Balahoju, Yogesh Kumar Maurya, Piotr J. Chmielewski, Tadeusz Lis, Mateusz Kondratowicz, Joanna Cybińska, and Marcin Stępień**

Abstract: Peripheral substitution of a π-extended porphyrin with bulky groups produces a curved chromophore with four helical stereogenic units. The curvature and stereochemistry of such porphyrins can be controlled by varying the substituents, coordinated metal ions, and apical ligands. In particular, when the achiral saddle-shaped free bases are treated with large metal ions, i.e., Cd^{II} or Hg^{II}, the resulting complexes convert to chiral propeller-like configurations. X-ray diffraction analyses show that apical coordination of a water molecule is sufficient to induce a notable bowl-like distortion of the cadmium complex, which however retains its chiral structure. For phenyl- and tolyl-substituted derivatives, the conversion is thermodynamically controlled, whereas complexes bearing bulky 4-(*tert*-butyl)phenyl groups transform into their chiral forms upon heating. In the latter case, the chiral Hg porphyrin was converted into the corresponding free base and other metal complexes without any loss of configurational purity, ultimately providing access to stable, enantiopure porphyrin propellers.

Introduction

Introduction of chirality into large π-aromatic molecules, such as nanocarbons[1–4] or porphyrinoids,[5] can produce unique optical characteristics ranging from extreme specific optical rotation values,[6] through amplified circular dichroism,[7] to exceptional circularly polarized luminescence.[8,9] Ongoing research on chiral aromatics explores their utility as e.g. catalysts,[10–15] switches,[16,17] receptors,[18,19] self-assembling motifs,[20–23] semiconductors,[24] and emissive materials.[25,26] Chiral features useful for supramolecular interactions can be introduced into aromatic molecules by substitution with groups containing stereocenters. However, intrinsic chiral distortion of π-aromatic surfaces, which strongly affects chromophore properties, is more efficiently induced by steric congestion of peripheral substituents or fused rings,[27] or by combining persistent curvature with appropriate topology of the ring system.[28,29] In systems containing several such stereogenic units, such as multi-helicene nanocarbons,[3,4] stereoisomer distribution is either not controllable,[30–47] or is predetermined by use of homochiral building blocks.[48] Post-synthetic modulation of stereochemistry is typically restricted to a single π-conjugated stereogen,[16,17] and it is generally difficult to achieve concerted stereocontrol over multiple sites in large aromatic molecules. While examples of thermodynamic equilibration are known,[37,49] π-conjugated systems that will change diastereomer populations in response to a stimulus remain rare.[50,51]

Looking for new designs of chiral aromatics, we considered sterically overcrowded porphyrins containing peripherally fused naphthalimide (NMI) subunits (Figure 1A). Porphyrin macrocycles have highly moldable shapes, which can be tuned by peripheral substitution and metal coordination.[52] Chirality in porphyrins and metalloporphyrins has been typically introduced with dissymmetric substituents or apical ligands, or by simultaneous desymmetrization of the substitution pattern and axial ligation.[5] In the present design, the stereochemistry of the macrocycle is controlled by bulky non-stereogenic groups (R, Figure 1A, B) placed at a distance from the core, i.e., at the outer NMI units.[43] We show that upon coordination of judiciously chosen metal ions, these structures can convert between the achiral saddle-shaped isomers, previously observed in *meso*-substituted NMI porphyrins,[53] and chiral, propeller-shaped isomers. Depending on the bulk of the R groups, the transformation can occur spontaneously, or upon additional thermal activation.

Results and Discussion

Symmetry Considerations

Metalloporphyrins **1**-M, **2**-M and **3**-M containing in-plane coordinated ions such as Zn^{II} can form two achiral (meso) isomers, with D_{2d} and C_{2h} point symmetries, respectively, and two enantiomer pairs with different symmetries, D_4 and C_2, respectively (Figure 1C, D). Each of these four symme-

[*] Dr. S. A. Balahoju, Dr. Y. K. Maurya, Prof. P. J. Chmielewski, Prof. T. Lis, M. Kondratowicz, Dr. J. Cybińska, Prof. M. Stępień
Wydział Chemii, Uniwersytet Wrocławski,
ul. F. Joliot-Curie 14, 50-383 Wrocław (Poland)
E-mail: marcin.stepien@uwr.edu.pl
Dr. J. Cybińska
(PORT) Polski Ośrodek Rozwoju Technologii,
ul. Stabłowicka 147, 54-066 Wrocław (Poland)

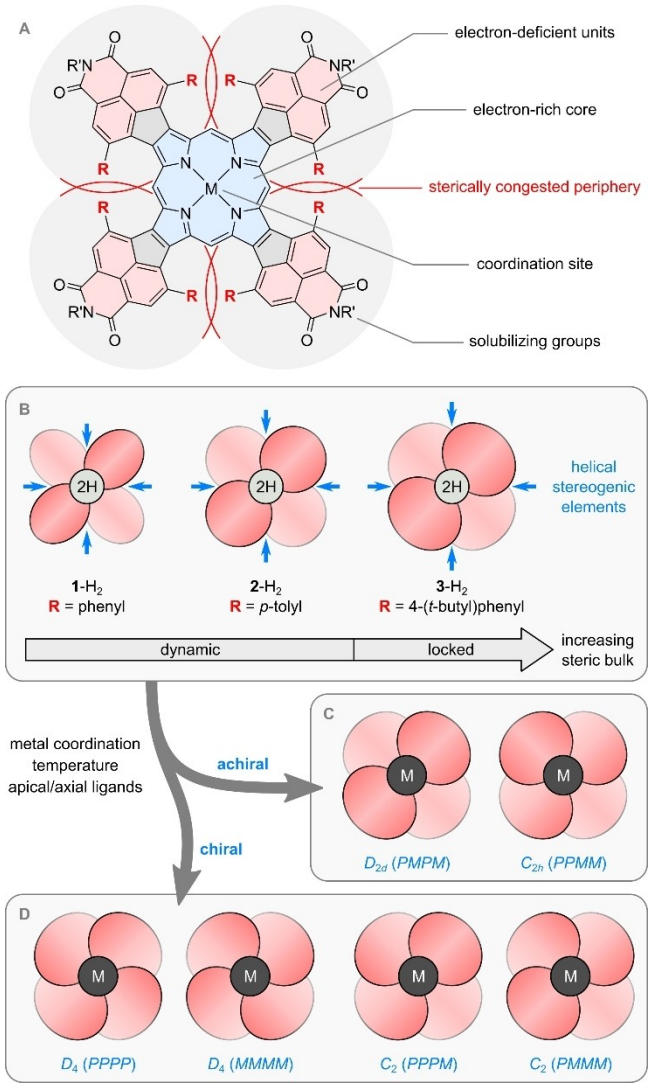

Figure 1. Structure and stereochemistry of heavily substituted porphyrin-ryleneimides. R′ = dipp = 2,6-diisopropylphenyl in **1**-M, **2**-M and **3**-M. R′ = Me in **1**′-M, **2**′-M, and **3**′-M (DFT only).

tries (PG_{max} in Table 1) can be unequivocally distinguished by counting the ^1H NMR signals of (a) meso protons, (b) isopropyl CH signals (n_{iPr}) of the rotationally locked R′ substituents, and (c) signals of the bulky R substituents (n_R), e.g., the *p*-Me resonances in **2**-M and **3**-M. These three signal counts are labeled respectively n_{meso}, n_{iPr}, and n_R in Table 1. In the free bases, the actual molecular symmetry is lower (PG_{fb}), however, because of rapid tautomerization in solution, the NMR symmetry observed at room temperature is identical with PG_{max}. Similarly, rapid pseudoinversion of sitting-atop/square-pyramidal complexes (e.g. with $M = Hg^{II}$) or ligand exchange in apically coordinated species (e.g. $M = Zn^{II}$(pyridine)) will result in an increase of observed symmetry from PG_{sa} to PG_{max}. For simplicity, we will use PG_{max} as stereochemistry descriptors, even if the molecular symmetry of a given species is lower.

Dynamic Systems

We commenced by synthesizing free-base porphyrins **1**-H_2 and **2**-H_2, containing respectively phenyl and *para*-tolyl substituents R. The two macrocycles were prepared from monopyrroles **4a** and **4b**, each available in 8 steps from acenaphthene,[43] and transformed into the corresponding zinc(II) complexes, **1**-Zn and **2**-Zn (Scheme 1). The steric bulk of R groups in monopyrroles **4a** and **4b** was previously found to ensure stereospecific formation and configurational stability of hexapyrrolohexaazacoronenes (HPHACs).[43] However, because the overlap of adjacent R groups in porphyrins is smaller than in the corresponding HPHACs (which contain six rather than four pyrrole units around the periphery), we anticipated that helix inversion barriers in porphyrins may be lower, permitting equilibration of stereoisomers at room temperature. The ^1H NMR spectrum of **1**-H_2 revealed a single species with D_{2d} symmetry, indicating that the phenyl derivative prefers an achiral saddle-shaped structure similar to those of the *meso*-substituted NMI porphyrins.[53] In contrast, the tolyl-substituted **2**-H_2 forms a mixture of stereoisomers consisting of 65 % D_{2d}, 21 % *rac*-C_2, and 14 % *rac*-D_4 (Scheme 1). The predominant stereoisomer D_{2d}-**2**-H_2 was isolated in the solid state (Figure 2),[54] where it showed a noticeable saddle-like distortion. The saddling parameter[55] for the porphyrin substructure in D_{2d}-**2**-H_2 (2.78 Å, Table S1) is comparable with values observed for *meso*-aryl NMI porphyrins (2.9–3.0 Å).[53] The vertical extent of the π system of D_{2d}-**2**-H_2 is however significantly smaller (5.73 Å, Figure 2, vs. ca. 9.0 Å in *meso*-aryl NMI porphyrins), reflecting a more flattened arrangement of NMI units in the present system.

Table 1: Isomerism and point symmetry groups (PGs) of **1**-M, **2**-M, and **3**-M.

Configuration[a]	PG_{max}[b]	n_{meso}[c]	n_{NMI}[c]	n_{iPr}[c]	n_R[c]	PG_{fb}[d]	PG_{sa}[e]
PMPM	D_{2d}	1	1	2	1	C_{2v}	C_{2v}
PPMM	C_{2h}	1	2	3[f]	2	C_s	C_s
PPPP, *MMMM*	D_4	1	1	1	1	D_2	C_4
PPPM, *PMMM*	C_2	3[f]	4[g]	4[g]	4[g]	C_1	C_1

[a] Local helicities around the periphery as defined in Figure 1C, D. [b] Maximum point symmetry group (square-planar coordination). [c] Number of equivalence classes (within PG_{max}) for meso, naphthalene (NMI), and isopropyl CH protons, and R substituents, respectively. [d] Point symmetry of the free base (M = 2 H, trans tautomer). [e] Point symmetry of sitting-atop complexes (e.g. $M = Hg^{II}$), and complexes with an apical ligand. [f] 1 : 1 : 2 intensity ratio. [g] 1 : 1 : 1 : 1 intensity ratio.

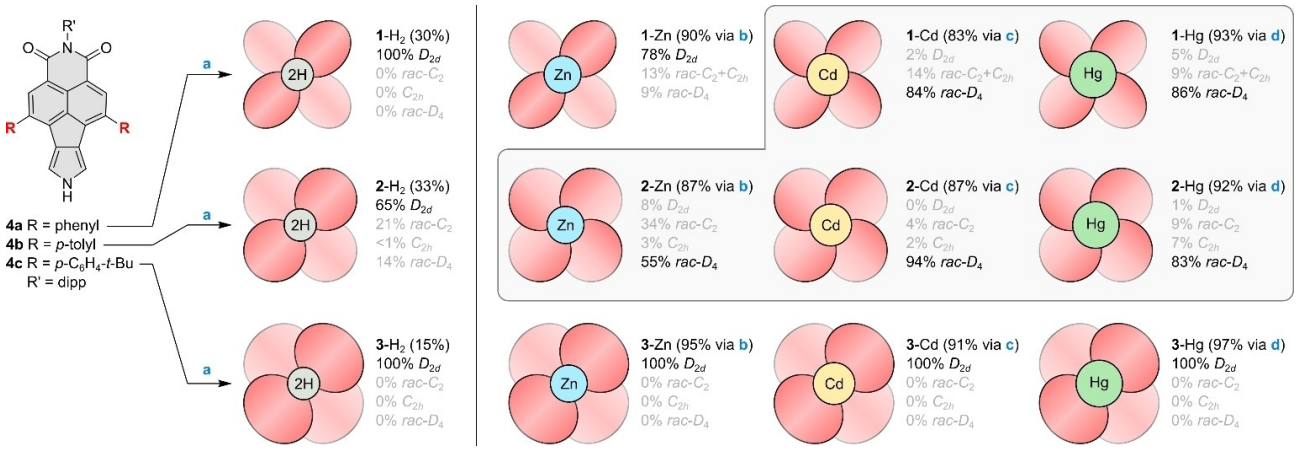

Scheme 1. Synthetic work. Reagents and conditions: a) i) paraformaldehyde, *p*-TSA, rt, 12 h, darkness, ii) DDQ, 1 h, reflux; b) $Zn(OAc)_2{\cdot}2\,H_2O$, $CHCl_3$/MeOH, 1 h, reflux; c) $Cd(OAc)_2{\cdot}H_2O$, pyridine or pyridine-d_5, 10 min, reflux; d) $Hg(OAc)_2$, pyridine or pyridine-d_5, rt, 10 min. Isolated yields are given for all compounds. Isomer fractions are estimated by integration of ^{1}H NMR meso resonances (300 K, $CDCl_3$ or CD_2Cl_2). In **1**-Zn, **1**-Cd, and **1**-Hg, *rac*-C_2 and C_{2h} forms are in fast exchange and yield one broad meso signal.

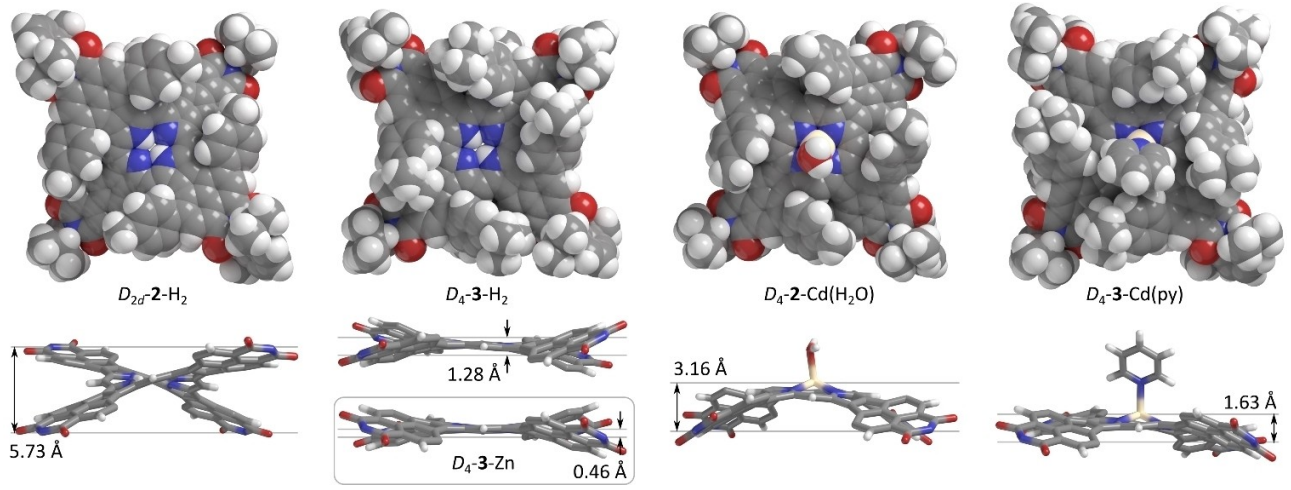

Figure 2. Molecular structures of selected porphyrins and metalloporphyrins determined using X-ray diffraction (XRD) analysis. Solvent molecules and disordered groups are removed for clarity. In the bottom projections R and R′ substituents are hidden to reveal distortions of the NMI-porphyrin cores. For D_{2d}-**2**-H_2, D_4-**3**-H_2, and D_4-**3**-Zn, the vertical extent of the π system is calculated from the displacements of imide N atoms relative to their mean plane. For D_4-**2**-Cd(H_2O) and D_4-**3**-Cd(py) the bowl depth is calculated as the distance between the Cd ion and the mean plane of the imide N atoms.

Remarkably, in comparison with the free bases **1**-H_2 and **2**-H_2, the corresponding zinc(II) complexes showed an increased preference for the propeller-like chiral D_4 structure, which constituted respectively 9 % and 55 % of the isomer mixtures of **1**-Zn and **2**-Zn. A ^{1}H ROESY spectrum measured for **2**-Zn ($CDCl_3$, 300 K, Figures S14, S15) revealed a dynamic behavior that is thought to be representative for the entire family of porphyrins and their complexes. In particular, an array of intense exchange (EXSY) correlations was observed among the four meso resonances of the *rac*-C_2 species and the single meso signal of the C_{2h} form. No chemical exchange was however observable for *meso*-H signals of the D_{2d} and *rac*-D_4 species, even if the temperature was raised to 330 K. At this temperature, significant line broadening was seen for C_2 and C_{2h}, whereas the signals of D_{2d} and *rac*-D_4 remained narrow, in line with the 300 K EXSY data. Exchange involving D_{2d} and D_4 structures is apparently too slow at these temperatures to be observable using EXSY spectroscopy, but it is nevertheless sufficiently fast to ensure equilibration of all species in solution. For the less hindered **1**-Zn, the dynamics are apparently more rapid: the *rac*-C_2 and C_{2h} forms are in fast exchange at room temperature, yielding a single, dynamically averaged meso resonance, which produces an EXSY cross-peak to the D_4 meso signal. These observations indicate that the dynamics follow the pattern shown in Scheme 2. The achiral structure C_{2h}, with the *PPMM* stereochemistry provides an inversion pathway between the two C_2 enantiomers *PPPM* and *PMMM*. Each of these two enantiomers can further isomerize to either the correspond-

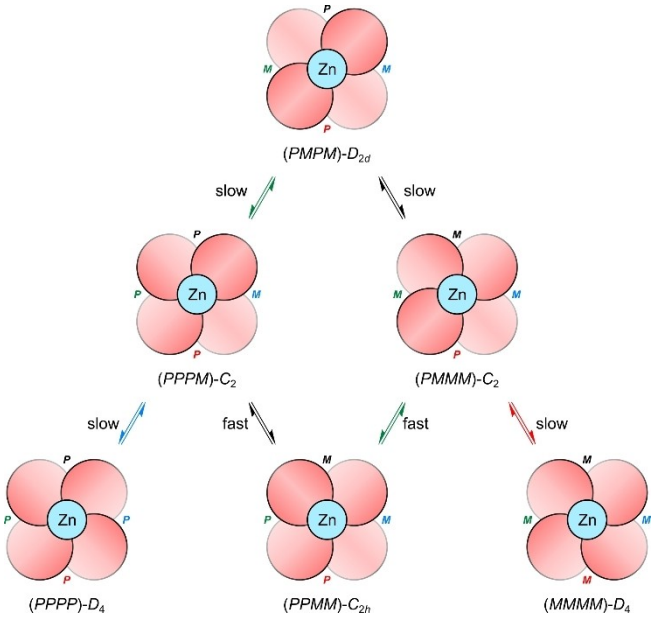

Scheme 2. Chirality dynamics of **2**-Zn. Arrows are color-coded to indicate the helical site undergoing inversion.

ing D_4 enantiomer, *PPPP* or *MMMM*, respectively, or to the achiral D_{2d} (*PMPM*) structure. The C_2–C_{2h} transformation is unique because the helical site undergoing inversion is located between two sites of opposite handedness, whereas in the C_2–D_4 and C_2–D_{2d} transformations, the inverted site is located between two sites of identical handedness. This difference may account for the experimentally observed lower energy barrier of C_2–C_{2h} exchange.

The above experiments indicated that (a) an appropriate choice of coordinated metal cation may determine the stereochemistry of the porphyrin ligand and (b) introduction of bulkier R groups at the periphery may increase inversion barriers and enhance configurational stability of the macrocycles. Changing the ionic radius seemed the simplest way to test the first hypothesis, given the known effect of ion size on metalloporphyrin conformations.[52] While the interplay between the metal-induced distortions and the unusual steric interactions at the periphery of our porphyrins was difficult to predict, we chose to increase the metal radius in **1**-M and **2**-M complexes, hoping to shift the equilibrium toward the chiral structures. Cd^{II} and Hg^{II} ions were chosen because their effective ionic radii in tetracoordinate environments[56] (0.78 Å and 0.96 Å, respectively) are significantly larger than the radius of Zn^{II} (0.60 Å).

Insertion of cadmium(II) and mercury(II) into **1**-H_2 and **2**-H_2 occurred rapidly in refluxing pyridine, yielding in each case a mononuclear complex, as evidenced by mass-spectrometric analyses. We were pleased to find that for each complex, the mixture of isomers contained predominantly the chiral *rac*-D_4 species (83 % to 94 % according to ^{1}H NMR, Scheme 1). The large cadmium(II) and mercury(II)[57,58] ions are often found located above the macrocyclic plane in metalloporphyrins, either as "sitting-atop" tetracoordinate complexes,[59,60] or as tetragonal-pyramidal species with an additional apical ligand.[61] Room-temperature ^{1}H NMR spectra of **1**-Cd, **1**-Hg, **2**-Cd, and **2**-Hg correspond to the maximum possible molecular symmetry of all isomers (PG_{max}, Table 1), consistent with effective equivalence of the two sides of the macrocycle. However, at low temperatures, a more complicated spectral pattern emerged for each complex, in particular, the dominant isomer showed splitting of the NMI singlet into two resonances of equal intensity. The latter change, indicative of symmetry lowering from D_4 to C_4, is thought to be induced by restricted motion of the metal ion across the macrocyclic plane, or by reversible binding of an apical ligand. Indeed, when an excess of pyridine-d_5 was added to the sample of **2**-Cd, the decoalescence range in CD_2Cl_2 changed from 240–260 K to 200–210 K, suggesting possible involvement of apical ligation.

Further evidence for ligand binding came from an XRD analysis of D_4-**2**-Cd, which revealed a water molecule apically coordinated to the Cd center (Figure 2). The off-axis tilt of the Cd–O bond and its length (2.31 Å) suggest that the ligand is rather weakly bound. Remarkably, coordination of the Cd(H_2O) moiety by the porphyrin produces a very pronounced bowl-shaped distortion of the macrocycle, with an apparent bowl depth exceeding 3 Å. The curvature is induced by the mismatch between the ionic radius and the diameter of the macrocyclic core, which can occasionally result in dramatic deformations in oligopyrrolic macrocycles.[62] A very significant doming distortion component of 0.822 Å was determined for D_4-**2**-Cd(H_2O) (Table S1).[55] The latter value is much larger than typically observed in pentacoordinate Cd^{II} porphyrins, in which it rarely exceeds 0.5 Å. This level of flexibility is remarkable, given the extent of substituent interdigitation at the periphery of the macrocycle. The bowl-shaped porphyrin core in D_4-**2**-Cd(H_2O) is not stereogenic, and the stereochemistry of the complex is solely determined by the four outer helices. However, local bowl chirality[63,29,47] could in principle be achieved in Etio-I-type porphyrin derivatives, e.g. ones bearing different R groups on each NMI subunit.

Locked Systems

Molecular modeling indicated that the bulkier 4-(*tert*-butyl)phenyl substituents might impart greater configurational stability to the porphyrins, potentially enabling separation of stereoisomers. The respective porphyrin, **3**-H_2 formed in lower yield than its less encumbered siblings **1**-H_2 and **2**-H_2, possibly because of the greater steric congestion of peripheral substituents. **3**-H_2 formed as the pure D_{2d} isomer, quite likely inheriting the stereochemistry of the initially formed porphyrinogen.[64] Metalation reactions, carried out as described for **1**-H_2 and **2**-H_2, took place with perfect stereospecificity, yielding pure D_{2d} isomers of **3**-Zn, **3**-Cd, and **3**-Hg. However, we suspected that the D_{2d} structures were actually kinetic reaction products, and a different isomer ratio might be attained under equilibrium conditions. This hypothesis was based on the previously observed differences in stereoisomer composition between the corresponding **1**-M and **2**-M systems, which we had

tentatively attributed to increased steric congestion around the macrocycle.

Indeed, we found that when D_{2d}-**3**-Zn was heated in toluene at 150 °C, it gradually isomerized into a mixture containing the chiral *rac*-D_4-**3**-Zn as the major component (64 %) and the equilibrium was reached after 4 days (Figure 3, Table 2). The final mixture contained no C_{2h} isomer, but it was observed as an intermediate after 12 h. A simplified procedure, in which the free base **3**-H_2 was heated with zinc(II) acetate in pyridine, gave a very similar result. Using the latter protocol, we were able to obtain isomer mixtures of **3**-Cd and **3**-Hg containing respectively 83 % and 85 % of the desired *rac*-D_4 isomer. In the absence of a metal source, the free base isomerized to a much smaller extent, with ca. 70 % of the D_{2d} isomer remaining after 96 h of heating.

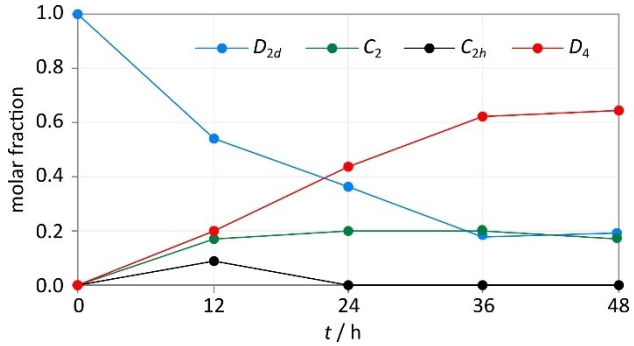

Figure 3. Isomerization of **3**-Zn (160 °C, toluene). The sample was isolated after each heating cycle, and the isomer ratio was established by integration of a ^{1}H NMR spectrum.

After high-temperature equilibration, the composition of isomer mixtures remained constant at room temperature. We found that *rac*-D_4-**3**-Hg could be separated from other isomers by repeated fractional crystallization, which provided the pure product in a 51 % isolated yield (Scheme 3). We took advantage of the inherent lability of mercury(II) porphyrins and transformed *rac*-D_4-**3**-Hg into the free base *rac*-D_4-**3**-H_2. The metal ion could be removed without loss of isomeric purity, by simply treating a dichloromethane solution of the Hg^{II} complex with 1 M aqueous HCl. Alternatively, the D_4 free base could be obtained by first demetalating the mixture of **3**-Hg isomers and subsequent fractional crystallization. *rac*-D_4-**3**-H_2 could then be stereospecifically converted into the corresponding zinc(II) and cadmium(II) complexes, *rac*-D_4-**3**-Zn and *rac*-D_4-**3**-Cd, respectively.

Racemic D_4-**3**-H_2 and D_4-**3**-Zn were characterized using XRD analysis, which confirmed the propeller-like configuration of peripheral substituents (Figure 2). In each structure, the NMI pyrrole units are noticeably twisted along their major axes, imparting a pronounced chiral distortion to the chromophore. Interdigitation of the bulky R groups results in much flatter aromatic cores than observed in D_{2d}-**2**-H_2, with the NMI units held closer to the mean macrocyclic plane. The vertical extent of the π system is particularly small in D_4-**3**-Zn (0.46 Å), possibly reflecting the rigidifying effect of metal coordination. The porphyrin substructures in D_4-**3**-H_2 and D_4-**3**-Zn show a combination of "propellering" (0.48 Å) and saddling distortion (0.48–

Table 2: Thermally induced isomerization of **3**-M.

System	Solvent	T [°C]	t [h]	D_{2d} [%]	C_2 [%]	C_{2h} [%]	D_4 [%]
3-H_2	pyridine-d_5[a]	130	96	≈70	[d]	[d]	[d]
3-Zn	toluene[b]	150	48	19	17	0	64
3-Zn	pyridine-d_5[a,c]	130	86	19	21	0	60
3-Cd	pyridine-d_5[a,c]	130	48	4	13	0	83
3-Hg	pyridine-d_5[a,c]	130	48	6	6	3	85

[a] Isomer distribution determined in situ. [b] Starting from D_{2d}-**3**-Zn, isomer distribution determined after isolation. [c] Starting from D_{2d}-**3**-H_2 and the corresponding metal acetate [d] Not assigned.

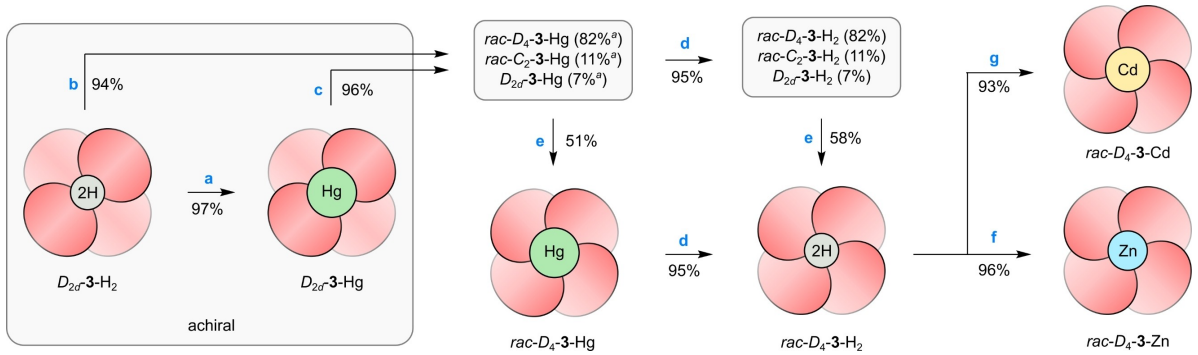

Scheme 3. Metalation chemistry of **3**-H_2. Reagents and conditions: a) $Hg(OAc)_2$, pyridine-d_5, rt, 10 min; b) $Hg(OAc)_2$, pyridine-d_5, 130 °C, 2×24 h, then basic alumina/DCM; c) 130 °C, 2×24 h, then basic alumina/DCM; d) 1 M HCl, DCM; e) fractional crystallization (DCM/hexane, 2 cycles); f) $Zn(OAc)_2{\cdot}2H_2O$, $CHCl_3$/MeOH, reflux, 1 h; g) $Cd(OAc)_2{\cdot}2H_2O$, pyridine-d_5, reflux, 10 min. [a] Isomer distribution for route (b) after isolation.

0.51 Å, Table S1).[55] The cadmium analogue was isolated in the solid state in the form of D_4-**3**-Cd(py), with a pyridine ligand bound apically to the metal center. The doming distortion in this species is much smaller than in D_4-**2**-Cd(H_2O). Apparently, the difference is caused by the greater size of R groups in the former complex, which become more congested on the concave side of the bowl.

Electronic Properties

Porphyrin systems **1**-M, **2**-M and **3**-M absorb strongly up to ca. 900 nm, with weak tailing absorptions reaching up to 1000 nm (Figure 4 and Figures S6–S10). They feature more intense Q-type bands in the NIR range and reduced electronic gaps in comparison with the previously reported NMI porphyrin derivatives.[53] These differences can be ascribed to substitution effects; in particular, the absence of *meso*-aryl groups in the present systems enables greater planarization of the chromophore. Furthermore, the R groups make significant contributions to the frontier molecular orbitals of **1**-M, **2**-M, and **3**-M, thus effectively extending the π system. In particular, for D_4-**3′**-Zn (Table S4), the average R group contribution is 24 % for the five highest occupied levels and 6 % for the five lowest unoccupied levels. Absorption spectra of the configurationally locked chromophores, **3**-H_2, **3**-Zn, **3**-Cd, and **3**-Hg, show remarkable dependence on the stereochemistry. While the absorption onsets are similar for the D_{2d} and D_4 configurations, the latter isomers show narrower bands with differently located maxima. These differences are most significant for **3**-Cd and **3**-Hg, wherein they may correspond to specific conformational effects caused by sitting-atop coordination of large metal ions. TD-DFT calculations performed for **3′**-H_2 and **3′**-Zn indicate that lowest-energy transitions in these systems arise through mixing of multiple excitations and should be more intense for D_4 isomers, as indeed observed experimentally (cf. Supporting Information).

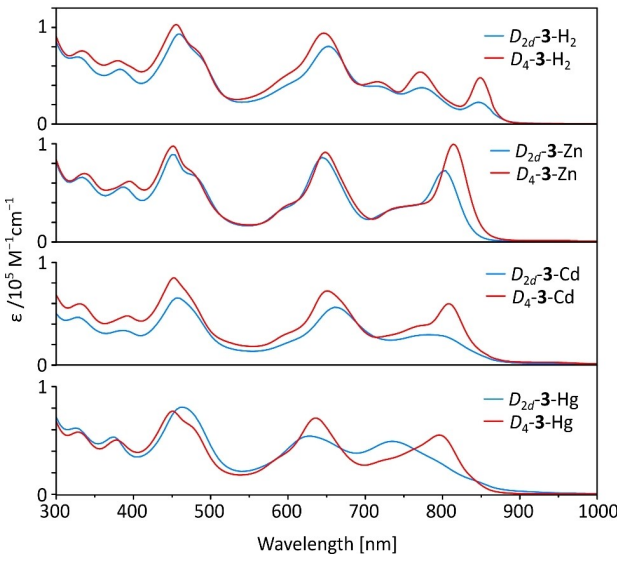

Figure 4. Absorption spectra of D_{2d} and D_4 isomers of **3**-M complexes (M = 2 H, Zn, Cd, and Hg, dichloromethane).

Fluorescence spectra recorded for isomerically pure D_{2d}- and *rac*-D_4-**3**-M (M = 2H, Zn, Cd) revealed weak near-infrared emissions (QY < 0.5 %), slightly dependent on the stereochemistry of the porphyrin and its metalation status (Figure S11, Table S3). The emission spectrum of *rac*-D_4-**3**-H_2 is notable for the narrow 0–0 band (λ_{max}^{em} = 855 nm, FWHM ≈ 37 nm) and relatively weak higher vibronic components. In comparison, the spectra of D_{2d}-**3**-H_2 and the Zn and Cd complexes are slightly broadened, but their overall appearance is similar. The small Stokes shifts imply that these large chromophores do not change their geometries significantly in the S1 state, possibly reflecting the rigidifying effect of bulky peripheral substitution.

Additional insight into the electronic structure of **3**-M derivatives was obtained from cyclic and differential pulse voltammetry measurements (Figures S1, S2, Table S2). The D_{2d}-**3**-H_2 free base undergoes the first electrochemical oxidation at 0.67 V (vs. Fc^+/Fc) and features six reversible reductions in the −1.02 V to −1.87 V potential range. These features, which correspond to a small electrochemical HOMO–LUMO gap (HLG) of 1.69 V, reflect the fusion of an electron-rich porphyrin core with multiple NMI subunits. In comparison, the isomeric *rac*-D_4-**3**-H_2 shows a small cathodic relocation of all reduction potentials and an anodic shift of the oxidation potentials, leading to an increase of the HLG to 1.74 V. Interestingly, the electrochemical HLGs of the D_{2d}-**3**-Zn and *rac*-D_4-**3**-Zn complexes are smaller than those of the corresponding free bases (1.67 V and 1.63 V, respectively), in contrast to the HLGs observed in the experimental and TD-DFT absorption spectra.

Chiroptical Properties

Initial experiments showed that cadmium(II) and mercury(II) complexes were easily demetalated and were partly decomposed during chiral chromatography. Separation of enantiomers was thus only attempted for selected free bases and zinc(II) complexes. The isomeric mixture of **2**-Zn showed partial separation on a chiral HPLC column yielding fractions with measurable circular dichroism (CD) spectra (Figures S3–S5). The rapid exchange between C_2 and C_{2h} isomers of **2**-Zn, observed by ^{1}H NMR (see above), indicated that racemization of the former species should be fast at room temperature. Thus, even though complete diastereomeric separation could not be achieved chromatographically, the entire intensity of the CD signal observed for HPLC fractions could be attributed to the enantiomeric excess of D_4.The gradual decay of the CD signal, occurring at room temperature with a half-life of $t_{1/2}$ = 29 min, reflects the isomerization rate of D_4, which is indeed slower than could be observed by EXSY spectroscopy.

In contrast to the stereochemically labile **2**-Zn, *rac*-D_4-**3**-H_2 and *rac*-D_4-**3**-Zn were separated into enantiomers, which did not racemize at room temperature. Their mirror-image CD spectra extended up to ca. 850 nm, showing multiple

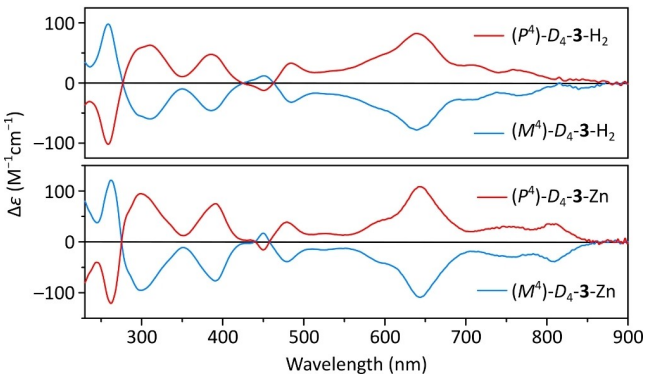

Figure 5. Circular dichroism spectra of enantiomeric pairs of D_4-**3**-H_2 and D_4-**3**-Zn (dichloromethane). Absolute stereochemistry was assigned on the basis of TD-DFT calculations.

Cotton effects in the UV, visible and near infrared ranges (Figure 5). Except for a change in NIR intensities, the CD spectra of the corresponding D_4-**3**-H_2 and D_4-**3**-Zn enantiomers are similar, indicating that the chiral features of the chromophore are not significantly affected by metal coordination. The experimental CD responses could be reliably reproduced in TD-DFT calculations, permitting unequivocal assignment of absolute configurations of the (P^4) and (M^4) enantiomers (Figures S40, S41). The presence of appreciable CD activity in the visible and NIR ranges of the spectrum indicates that even though the chiral distortion is induced by peripheral substitution it has a pronounced effect on the properties of the π system. This effect may originate not only from the propeller distortion of the NMI porphyrin chromophore but also from the MO admixing of the helically arranged R substituents (vide supra).

Conclusion

We have shown here that by suitably engineering steric congestion around an electron-deficient π-extended porphyrin, it is possible to create chiral NIR-active chromophores. In the strategy presented herein, it is not necessary to introduce intrinsically chiral moieties, and the configuration of the chromophore is controlled by appropriate interdigitation of non-stereogenic substituents. Importantly, the chromophores can be transformed between achiral and chiral configurations by coordination of metal ions, with large ionic radii favoring the formation of chiral structures. The curvature of the π system is further tuned by apical coordination to the metal, which induces a significant bowl-shaped distortion. The latter effect may be used to affect curvature-dependent properties[65,66] with metal coordination, e.g., to induce self-assembly or host-guest complexation. The present strategy of stereocontrol is expected to work with more complicated substituents, containing additional chromophores or redox units, and may be applicable to other oligopyrrole macrocycles.

Acknowledgements

Financial support from the Foundation for Polish Science (TEAM POIR.04.04.00-00-5BF1/17-00) is gratefully acknowledged. Quantum-chemical calculations were performed in the Wrocław Center for Networking and Supercomputing.

Conflict of Interest

The authors declare no conflict of interest.

Data Availability Statement

The data that support the findings of this study are available in the Supporting Information of this article.

Keywords: Chirality · Coordination Chemistry · Metal Complexes · Porphyrins · Stereochemistry

[1] J. M. Fernández-García, P. J. Evans, S. Filippone, M. Á. Herranz, N. Martín, *Acc. Chem. Res.* **2019**, *52*, 1565–1574.
[2] I. G. Stará, I. Starý, *Acc. Chem. Res.* **2020**, *53*, 144–158.
[3] K. Kato, Y. Segawa, K. Itami, *Synlett* **2019**, *30*, 370–377.
[4] T. Mori, *Chem. Rev.* **2021**, *121*, 2373–2412.
[5] H. Lu, N. Kobayashi, *Chem. Rev.* **2016**, *116*, 6184–6261.
[6] M. Gingras, G. Félix, R. Peresutti, *Chem. Soc. Rev.* **2013**, *42*, 1007–1050.
[7] X. Xiao, S. K. Pedersen, D. Aranda, J. Yang, R. A. Wiscons, M. Pittelkow, M. L. Steigerwald, F. Santoro, N. J. Schuster, C. Nuckolls, *J. Am. Chem. Soc.* **2021**, *143*, 983–991.
[8] S. Sato, A. Yoshii, S. Takahashi, S. Furumi, M. Takeuchi, H. Isobe, *Proc. Natl. Acad. Sci. USA* **2017**, *114*, 13097–13101.
[9] Z. Qiu, C.-W. Ju, L. Frédéric, Y. Hu, D. Schollmeyer, G. Pieters, K. Müllen, A. Narita, *J. Am. Chem. Soc.* **2021**, *143*, 4661–4667.
[10] H.-Y. Thu, G. S.-M. Tong, J.-S. Huang, S. L.-F. Chan, Q.-H. Deng, C.-M. Che, *Angew. Chem. Int. Ed.* **2008**, *47*, 9747–9751; *Angew. Chem.* **2008**, *120*, 9893–9897.
[11] L.-M. Jin, X. Xu, H. Lu, X. Cui, L. Wojtas, X. P. Zhang, *Angew. Chem. Int. Ed.* **2013**, *52*, 5309–5313; *Angew. Chem.* **2013**, *125*, 5417–5421.
[12] C. Li, K. Lang, H. Lu, Y. Hu, X. Cui, L. Wojtas, X. P. Zhang, *Angew. Chem. Int. Ed.* **2018**, *57*, 16837–16841; *Angew. Chem.* **2018**, *130*, 17079–17083.
[13] F. Burg, M. Gicquel, S. Breitenlechner, A. Pöthig, T. Bach, *Angew. Chem. Int. Ed.* **2018**, *57*, 2953–2957; *Angew. Chem.* **2018**, *130*, 3003–3007.
[14] K. Lang, S. Torker, L. Wojtas, X. P. Zhang, *J. Am. Chem. Soc.* **2019**, *141*, 12388–12396.
[15] Y. Hu, K. Lang, J. Tao, M. K. Marshall, Q. Cheng, X. Cui, L. Wojtas, X. P. Zhang, *Angew. Chem. Int. Ed.* **2019**, *58*, 2670–2674; *Angew. Chem.* **2019**, *131*, 2696–2700.
[16] H. Isla, J. Crassous, *C. R. Chim.* **2016**, *19*, 39–49.
[17] P. Ravat, T. Šolomek, M. Juríček, *ChemPhotoChem* **2019**, *3*, 180–186.
[18] M. Sapotta, P. Spenst, C. R. Saha-Möller, F. Würthner, *Org. Chem. Front.* **2019**, *6*, 892–899.
[19] M. Weh, J. Rühe, B. Herbert, A.-M. Krause, F. Würthner, *Angew. Chem. Int. Ed.* **2021**, *60*, 15323–15327; *Angew. Chem.* **2021**, *133*, 15451–15455.

[20] R. van Hameren, A. M. van Buul, M. A. Castriciano, V. Villari, N. Micali, P. Schön, S. Speller, L. Monsù Scolaro, A. E. Rowan, J. A. A. W. Elemans, R. J. M. Nolte, *Nano Lett.* **2008**, *8*, 253–259.
[21] P. Iavicoli, H. Xu, L. N. Feldborg, M. Linares, M. Paradinas, S. Stafström, C. Ocal, B. Nieto-Ortega, J. Casado, J. T. López Navarrete, R. Lazzaroni, S. D. Feyter, D. B. Amabilino, *J. Am. Chem. Soc.* **2010**, *132*, 9350–9362.
[22] F. Helmich, C. C. Lee, A. P. H. J. Schenning, E. W. Meijer, *J. Am. Chem. Soc.* **2010**, *132*, 16753–16755.
[23] C. Oliveras-González, F. Di Meo, A. González-Campo, D. Beljonne, P. Norman, M. Simón-Sorbed, M. Linares, D. B. Amabilino, *J. Am. Chem. Soc.* **2015**, *137*, 15795–15808.
[24] D. Reger, P. Haines, K. Y. Amsharov, J. A. Schmidt, T. Ullrich, S. Bönisch, F. Hampel, A. Görling, J. Nelson, K. E. Jelfs, D. M. Guldi, N. Jux, *Angew. Chem. Int. Ed.* **2021**, *60*, 18073–18081; *Angew. Chem.* **2021**, *133*, 18221–18229.
[25] D.-W. Zhang, M. Li, C.-F. Chen, *Chem. Soc. Rev.* **2020**, *49*, 1331–1343.
[26] C. M. Cruz, S. Castro-Fernández, E. Maçôas, J. M. Cuerva, A. G. Campaña, *Angew. Chem. Int. Ed.* **2018**, *57*, 14782–14786; *Angew. Chem.* **2018**, *130*, 14998–15002.
[27] M. Rickhaus, M. Mayor, M. Juríček, *Chem. Soc. Rev.* **2016**, *45*, 1542–1556.
[28] M. Rickhaus, M. Mayor, M. Juríček, *Chem. Soc. Rev.* **2017**, *46*, 1643–1660.
[29] Y. Wang, O. Allemann, T. S. Balaban, N. Vanthuyne, A. Linden, K. K. Baldridge, J. S. Siegel, *Angew. Chem. Int. Ed.* **2018**, *57*, 6470–6474; *Angew. Chem.* **2018**, *130*, 6580–6584.
[30] W. Yue, W. Jiang, M. Böckmann, N. L. Doltsinis, Z. Wang, *Chem. Eur. J.* **2014**, *20*, 5209–5213.
[31] X.-Y. Wang, X.-C. Wang, A. Narita, M. Wagner, X.-Y. Cao, X. Feng, K. Müllen, *J. Am. Chem. Soc.* **2016**, *138*, 12783–12786.
[32] D. Meng, H. Fu, C. Xiao, X. Meng, T. Winands, W. Ma, W. Wei, B. Fan, L. Huo, N. L. Doltsinis, Y. Li, Y. Sun, Z. Wang, *J. Am. Chem. Soc.* **2016**, *138*, 10184–10190.
[33] T. Fujikawa, Y. Segawa, K. Itami, *J. Am. Chem. Soc.* **2016**, *138*, 3587–3595.
[34] T. Katayama, S. Nakatsuka, H. Hirai, N. Yasuda, J. Kumar, T. Kawai, T. Hatakeyama, *J. Am. Chem. Soc.* **2016**, *138*, 5210–5213.
[35] Y. Hu, X.-Y. Wang, P.-X. Peng, X.-C. Wang, X.-Y. Cao, X. Feng, K. Müllen, A. Narita, *Angew. Chem. Int. Ed.* **2017**, *56*, 3374–3378; *Angew. Chem.* **2017**, *129*, 3423–3427.
[36] T. Hosokawa, Y. Takahashi, T. Matsushima, S. Watanabe, S. Kikkawa, I. Azumaya, A. Tsurusaki, K. Kamikawa, *J. Am. Chem. Soc.* **2017**, *139*, 18512–18521.
[37] V. Berezhnaia, M. Roy, N. Vanthuyne, M. Villa, J.-V. Naubron, J. Rodriguez, Y. Coquerel, M. Gingras, *J. Am. Chem. Soc.* **2017**, *139*, 18508–18511.
[38] Y. Zhu, Z. Xia, Z. Cai, Z. Yuan, N. Jiang, T. Li, Y. Wang, X. Guo, Z. Li, S. Ma, D. Zhong, Y. Li, J. Wang, *J. Am. Chem. Soc.* **2018**, *140*, 4222–4226.
[39] K. Kato, Y. Segawa, L. T. Scott, K. Itami, *Angew. Chem. Int. Ed.* **2018**, *57*, 1337–1341; *Angew. Chem.* **2018**, *130*, 1351–1355.
[40] U. Hahn, E. Maisonhaute, J.-F. Nierengarten, *Angew. Chem. Int. Ed.* **2018**, *57*, 10635–10639; *Angew. Chem.* **2018**, *130*, 10795–10799.
[41] N. J. Schuster, R. Hernández Sánchez, D. Bukharina, N. A. Kotov, N. Berova, F. Ng, M. L. Steigerwald, C. Nuckolls, *J. Am. Chem. Soc.* **2018**, *140*, 6235–6239.
[42] G. Liu, T. Koch, Y. Li, N. L. Doltsinis, Z. Wang, *Angew. Chem. Int. Ed.* **2019**, *58*, 178–183; *Angew. Chem.* **2019**, *131*, 184–189.
[43] M. Navakouski, H. Zhylitskaya, P. J. Chmielewski, T. Lis, J. Cybińska, M. Stępień, *Angew. Chem. Int. Ed.* **2019**, *58*, 4929–4933; *Angew. Chem.* **2019**, *131*, 4983–4987.
[44] X. Guo, Z. Yuan, Y. Zhu, Z. Li, R. Huang, Z. Xia, W. Zhang, Y. Li, J. Wang, *Angew. Chem. Int. Ed.* **2019**, *58*, 16966–16972; *Angew. Chem.* **2019**, *131*, 17122–17128.
[45] Y. Wang, Z. Yin, Y. Zhu, J. Gu, Y. Li, J. Wang, *Angew. Chem. Int. Ed.* **2019**, *58*, 587–591; *Angew. Chem.* **2019**, *131*, 597–601.
[46] Y. Zhu, X. Guo, Y. Li, J. Wang, *J. Am. Chem. Soc.* **2019**, *141*, 5511–5517.
[47] K. Kise, S. Ooi, H. Saito, H. Yorimitsu, A. Osuka, T. Tanaka, *Angew. Chem. Int. Ed.* **2022**, *61*, e202112589; *Angew. Chem.* **2022**, *134*, e202112589.
[48] F. Zhang, K. Radacki, H. Braunschweig, C. Lambert, P. Ravat, *Angew. Chem. Int. Ed.* **2021**, *60*, 23656–23660; *Angew. Chem.* **2021**, *133*, 23848–23852.
[49] C. Weiss, D. I. Sharapa, A. Hirsch, *Chem. Eur. J.* **2020**, *26*, 14100–14108.
[50] J. C. M. Kistemaker, P. Štacko, J. Visser, B. L. Feringa, *Nat. Chem.* **2015**, *7*, 890–896.
[51] K. K. Kartha, A. Takai, Z. Futera, J. Labuta, M. Takeuchi, *Angew. Chem. Int. Ed.* **2021**, *60*, 16466–16471; *Angew. Chem.* **2021**, *133*, 16602–16607.
[52] C. J. Kingsbury, M. O. Senge, *Coord. Chem. Rev.* **2021**, *431*, 213760.
[53] H. Zhylitskaya, J. Cybińska, P. Chmielewski, T. Lis, M. Stępień, *J. Am. Chem. Soc.* **2016**, *138*, 11390–11398.
[54] Deposition Numbers 2121158, 2121169, 2121177, 2121186, and 2121182 contain the supplementary crystallographic data for this paper. These data are provided free of charge by the joint Cambridge Crystallographic Data Centre and Fachinformationszentrum Karlsruhe Access Structures service.
[55] J. Krumsieck, M. Bröring, *Chem. Eur. J.* **2021**, *27*, 11580–11588.
[56] R. D. Shannon, *Acta Crystallogr. Sect. A* **1976**, *32*, 751–767.
[57] J. K. M. Sanders, N. Bampos, Z. Clyde-Watson, S. L. Darling, J. C. Hawley, H.-J. Kim, C. C. Mak, S. J. Webb in *The Porphyrin Handbook, Vol. 3* (Eds.: K. Kadish, K. M. Smith, R. Guilard), Elsevier, Amsterdam, **2000**, pp. 1–112.
[58] C. M. Lemon, P. J. Brothers, B. Boitrel, *Dalton Trans.* **2011**, *40*, 6591–6609.
[59] A. Hazell, *Acta Crystallogr. Sect. C* **1986**, *42*, 296–299.
[60] M.-C. Wang, L.-S. Sue, B.-C. Liau, B.-T. Ko, S. Elango, J.-H. Chen, *Inorg. Chem.* **2001**, *40*, 6064–6068.
[61] P. F. Rodesiler, E. A. H. Griffith, N. G. Charles, L. Lebioda, E. L. Amma, *Inorg. Chem.* **1985**, *24*, 4595–4600.
[62] T. Yonezawa, S. A. Shafie, S. Hiroto, H. Shinokubo, *Angew. Chem. Int. Ed.* **2017**, *56*, 11822–11825; *Angew. Chem.* **2017**, *129*, 11984–11987.
[63] M. A. Petrukhina, K. W. Andreini, L. Peng, L. T. Scott, *Angew. Chem. Int. Ed.* **2004**, *43*, 5477–5481; *Angew. Chem.* **2004**, *116*, 5593–5597.
[64] Y.-D. Wu, D.-F. Wang, J. L. Sessler, *J. Org. Chem.* **2001**, *66*, 3739–3746.
[65] S. Mizyed, P. E. Georghiou, M. Bancu, B. Cuadra, A. K. Rai, P. Cheng, L. T. Scott, *J. Am. Chem. Soc.* **2001**, *123*, 12770–12774.
[66] M. Saito, H. Shinokubo, H. Sakurai, *Mater. Chem. Front.* **2018**, *2*, 635–661.

Manuscript received: January 16, 2022
Accepted manuscript online: February 7, 2022
Version of record online: February 24, 2022